JJEE
Volume 7, Number 3, September 2021
Pages 265-287
Jordan Journal of Electrical Engineering
ISSN (Print): 2409-9600, ISSN (Online): 2409-9619

Logarithmically-Wound Helix Antenna Excited for Axial-Mode Operations

Ayotunde Ayorinde[1], Sulaiman Adeniyi Adekola[2], A. Ike Mowete[3*]

[1, 3] Department of Electrical and Electronics Engineering, University of Lagos, Akoka, Lagos, Nigeria
E-mail: amowete@unilag.edu.ng
[2] Department of Electrical and Electronics Engineering, Federal University of Technology, Otuoke, Nigeria

Received: February 22, 2021 *Revised: April 06, 2021* *Accepted: April 14, 2021*

***Abstract*—** In this paper, the axial-mode performance features of a non-uniform helix, whose non-uniformity is defined by a logarithmic variation of turns spacing along its axis, is presented. Using the classical vector potential approach, the paper rigorously formulates radiation-zone field integrals for the antenna in terms of an unknown distribution of current. Because the formulation derives from a comprehensive analytical description of this 'log-helix' antenna's geometry, the unknown current distribution is readily determined with the use of the circuit-geometric properties of the Method of Moments (MoM). Subsequently, computational results reveal that - as obtained with other non-uniform helical antennas - the 'log-helix' antenna performs significantly better than the corresponding uniform helical antenna of identical axial length. As examples, a 39% increase in power gain was recorded for the log-helix over the corresponding uniform helix; whilst a 25% improvement in radiation field's axial ratio was achieved. In addition to far-zone fields and their associated performance metrics, antenna input parameters are also computed and discussed in details in this paper. Outcomes of a comparison of the performance of the log-helix with that of an exponential helix of about the same axial profile suggest that whereas the latter has a better power gain performance, the former is superior in terms of axial ratio bandwidth performance.

Keywords – Axial mode; Logarithmic turns spacing; Non-uniform helical antenna.

1. INTRODUCTION

The helical antenna operated in the axial mode has attracted - over the years - quite a few practical applications on account of its inherent properties of circularly polarized radiation fields, wide bandwidth, impedance matching capabilities and associated broadband features [1, 2]. Many of these applications routinely require better performance characteristics than the conventional helical antenna of uniform geometry is ordinarily able to provide. As a consequence, a number of schemes have been developed for the purposes of attracting the desired performance improvement, particularly gain enhancement and axial ratio refinement [3, 4]. One of the earliest of such schemes was reported by Carver [4], who located the conventional helical antenna within a conical horn to obtain a gain response, four times as large as that of the conventionally oriented helix of the same axial length. Nakano et al. reported a significant enhancement of antenna 'power gain' through the introduction of a parasitic element, wound from a point located diametrically opposite 1½ turns of the driven element [3]. On the other hand, King and Wong showed - by experimentally and parametrically investigating the response of fixed-length, variable-diameter, variable-pitch angle helical antennas - that higher gains can be obtained through a reduction in pitch angle [5]. Fu et al. suggested that a linear variation in the helical antenna's pitch angle can enhance circular polarization and improve impedance matching capabilities [6].

* Corresponding author
Article's DOI: 10.5455/jjee.204-1614026886

In recent times, a number of helical antenna performance improvement schemes have focused on the introduction of non-uniformities into the antenna geometry. The contributions of Chen et al. revealed that exponentially varying the turns spacing of a fixed-diameter axial mode helical antenna can attract close to a 59% increase in axial ratio bandwidth [7]. Kononov and Balanis considered two cases of geometrical non-uniformity involving exponential tapering of the antenna structure: i) by allowing the diameter to vary linearly with ϕ and ii) with pitch angle kept constant in one case, and allowed to vary in another [8]. According to the results reported by them, antenna responses to variations in diameter are not 'well-behaved' when the pitch is kept constant, but are more systematic, if pitch is allowed to vary. Jimisha and Kumar also examined the effects of exponential non-uniformity on the performance of the axial-mode helical antenna, in this case, with the pitch angle characterized by an exponential variation along antenna axis, and through a modification of the 'pitch profile' with the use of Catmull-Rom spline functions [9]. Due to the introduction of this non-uniformity, a significant enhancement of gain was achieved. Of particular interest to this paper are the contributions by Elkamchouchi and Salem, who investigated the responses of the non-uniform axial mode helical antenna in which non-uniformities in antenna radius are of the linear, exponential, and logarithmic varieties [1, 10]. First, using a NECII modelling of the antenna feed as a 'delta-gap' generator without the conventional ground plane, they obtained simulation results that indicated that the 'exponential-helix' is the best performing of the three [1]. Then, in a companion publication, the authors included a ground plane and obtained a number of interesting simulation results, the more notable of which include the observation that whereas the 'exponential helix' remained the best performing of the three, the 'linear-helix' recorded an improved gain of 20 dB, which is better than the 17 dB recorded by the exponential helix, in the absence of the ground plane [10]. It was also observed by the authors [10] that in the case of the best performing 'exponential helix', gain - in general - increased with increase in pitch of the 'feeding section', and that when resistively or inductively loaded at its beginning, the best performance is recorded at a 'feeding section pitch' of 0.14λ.

Unlike the 'numerical experiments' approach that characterized the contributions in [1] and [10], a systematic approach was reported by Dinkic et al. [11], which focused on gain performance optimization of the non-uniform helical antenna defined by linear variations of antenna geometrical parameters (radius and pitch angle) along the antenna axis. The authors, informed by results of previous investigations, selected the helical geometry characterized by linearly varying parameters, for gain optimization. And the optimization algorithms utilized included a hybrid of the Neider-Mead simplex and particle swarm optimization (PSO) routines. Simulation results reported in the paper reveal that when located above a ground plane of infinite extent, the non-uniform helical antenna with linearly varying geometrical parameters records a gain of 2.5 dB greater than a uniform helical antenna of identical axial length. By creating a 2 x 2 array of the optimized non-uniform antennas, a gain enhancement of about 6 dB was reported in [12]. In a related publication, the authors - using the same optimization procedure - investigated the effects of conductor losses on the gain of the optimized non-uniform helical antenna [13]. In the main, the paper's simulation results indicate that there is a range of conductivities over which the gain performance of the optimized non-uniform helical antenna is markedly superior to that

of the optimized uniform helical antenna of the same dimensions. Outside this range, the results also suggest that the difference in gain performance of the two is minimal, so that the optimized uniform is to be preferred, on account of simplicity in design and construction. A genetic algorithm (GA) based optimization approach reported by Lovestead and Safaai-Jazi focused on a non-uniform helix, for which antenna non-uniformity is defined by a continuous variation of pitch angle over the extent of the helix's axial profile [14]. This non-uniformity - derived from the GA procedure - required the prescription of antenna geometry that simultaneously satisfies the constraints of maximum gain and minimum axial ratio. Important outcomes of the investigations include the fact that the GA-optimized non-uniform helical antenna's directivity is some 0.6 dB better than that of the corresponding uniform helical antenna and that the GA-optimized antenna is limited in bandwidth and axial ratio on the lower and higher frequency sides, respectively. It may be of interest to mention that the use of the helical antenna's non-uniformity towards the improvement of normal-mode operations has also attracted research attention in recent times. Examples include the contribution by Garakhili [15], in which two non-uniform (varying-pitch angle) normal-mode helical antennas were nested in the design of a dual-band radiating device, described as producing a 'fractional bandwidth' of 19.7%. Mahmood and Al-Dalawie also reported the design, construction, and performance evaluation of a non-uniform normal-mode helical antenna [16]. The antenna - designed with the use of an 'online helical antenna calculator' - recorded between 10-12 dB more in received power than the off-the-shelve antennas utilized for commercial broadcast TV reception in the UHF band.

Although the analysis of a logarithmic spiral antenna was reported by Thaysen et al. [17], there is no record - to the best of our knowledge - of any analysis involving the helical antenna characterized by a non-uniformity defined by a logarithmic variation of its turns spacing along its axis. Consequently, the main objective of this paper is to investigate the response of the axial-mode circular helical antenna of logarithmically varying turns spacing. First, the paper resolves the non-trivial problem of providing an analytical description for the log-helix geometry and, then, following the use of the vector potential procedure, the radiation field integrals of thin-wire log-helix - in which the axial current distribution is the only unknown quantity - are formulated. Next, and because the 'log-helix' is mounted on a ground plane of infinite extent, the image theory is invoked and utilized in conjunction with the method of moments to determine the unknown current and facilitate the compilation of computational data concerning the antenna's input characteristics and radiation-zone performance parameters.

The computational results show that the axial-mode log-helix is capable of achieving a 39% increase in gain over that of the corresponding uniformly wound helix and without loss of circular polarization properties. Also, for a particular choice of logarithmic variation factor denoted by β, a 25% improvement is recorded for axial ratio whose bandwidth is shown by the computational results to increase by 10% for certain values of β.

2. PROBLEM FORMULATION

The geometry problem of a thin-wire logarithmically-wound N-turn helix antenna characterized by a circular cross-section, mounted on a perfectly conducting ground plane of

infinite extent, is depicted in Fig. 1(a), while its image-theory-based equivalent is displayed in Fig. 1(b).

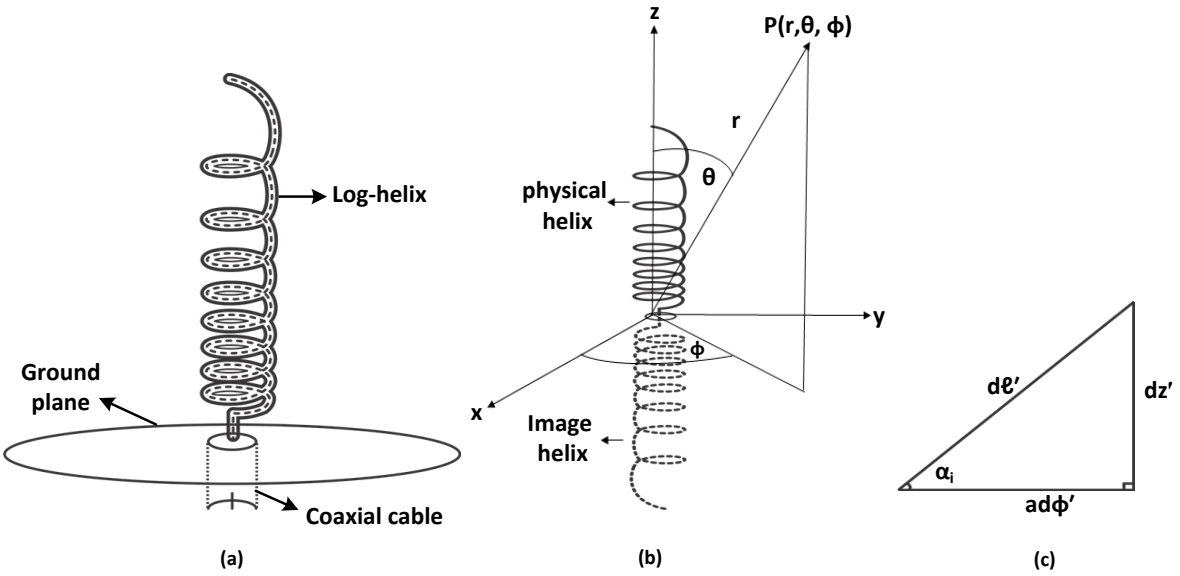

Fig. 1. a) A thin-wire log-helix mounted on a ground plane of infinite extent; b) an image-theory equivalent of the original geometry problem; c) a differential element of the log-helix rolled on a plane surface.

Without much difficulty, an exact analytical description of the geometry in terms of a position vector symbolized by $\bar{r}'$ and extending from the origin of the coordinate system to any point on the N-turn log-helical structure admits the form:

$$\vec{r}' = a\cos\phi'\hat{a}_x + a\sin\phi'\hat{a}_y + p\ln\left[\frac{\Phi_N}{\Phi_N - \beta\phi'}\right]\hat{a}_z, \qquad 0 \le \phi' \le 2\pi N \tag{1}$$

in which $\Phi_N = 2\pi N\beta + 1$, with 'a' standing for radius of the circular cross-section, and the parameters p and β, geometrically defining the logarithmic variation of turns spacing, $\hat{a}_x$, $\hat{a}_y$, $and\ \hat{a}_z$ are the usual unit vectors along the Cartesian coordinate axes, whilst ϕ' denotes the running angular variable along the log-helix structure. The parameters 'p' and 'β' appearing in Eq. (1) define the logarithmic variation of the antenna's turns spacing, and may be regarded as design variables prescribed by the following considerations. Now, for the uniformly wound helix, the variation along the z-axis is expressed as:

$$z' = (a\tan\alpha)\phi', \qquad 0 \le \phi' \le 2\pi\mathrm{N} \tag{2}$$

where α represents the pitch angle which remains constant throughout the extent of the uniform helix. In order to undertake a comparative performance analysis of the log-helix and the corresponding uniform helix, the practice in [1, 7] is followed to impose the design constraint of identical axial length for both helices. This constraint is met, in this case, when the parameter p featured in Eq. (1) is given by:

$$p = \frac{2\pi N a\tan(\alpha)}{\ln(2\pi N\beta + 1)}. \tag{3}$$

It is clear from Eq. (3) that the parameter β essentially defines the antenna's logarithmic variation and is consequently here referred to as the 'logarithmic variation factor'. To specify this factor, it is noted that when a differential element of the log-helix is rolled on a plane

surface, the geometry described by the illustration of Fig. 1(c) emerges, and from which it is easy to see that the pitch angle α_i of the log-helix is expressible as:

$$\alpha_i = \tan^{-1}\left(\frac{dz'}{ad\phi'}\right) \tag{4}$$

Since the z-component of a point on the log-helix is given by $z' = p\ln\left[\frac{\Phi_N}{\Phi_N - \beta\phi'}\right]$, the pitch angle α_i ultimately passes over to:

$$\alpha_i = \tan^{-1}\left(\frac{p\beta}{a\left(\Phi_N - \beta\phi'\right)}\right) \tag{4a}$$

which is clearly a function of the running variable ϕ' with the direct physical implication that the pitch angle is continuously varying along the log-helical geometry. Thus, the log-helix belongs to the class of non-uniform helical antennas, for which both turns spacing and pitch angle vary along antenna axis. The starting pitch angle α_s is deducible from Eq. (4a) by simply setting $\phi' = 0$, while the ending pitch angle α_e is attained when $\phi' = 2\pi N$; thus

$$\alpha_s = \tan^{-1}\left(\frac{p\beta}{a\left(2\pi N\beta + 1\right)}\right) \tag{4b}$$

and

$$\alpha_e = \tan^{-1}\left(\frac{p\beta}{a}\right) \tag{4c}$$

Towards determining the arm length of the log-helix, the differential length $d\ell'$ of the helical configuration may be expressed using the following well-known formula [18]:

$$dl' = \sqrt{\left(dx'\right)^2 + \left(dy'\right)^2 + \left(dz'\right)^2} = a\left(\sqrt{1 + \left[\frac{p\beta}{a\left(\Phi_N - \beta\phi'\right)}\right]^2}\right)d\phi', \tag{5}$$

which, when integrated from 0 to $2\pi N$ gives the total arm length L of the logarithmic helical antenna according to:

$$L = a\int_0^{2\pi N}\left(\sqrt{1 + \left[\frac{p\beta}{a\left(\Phi_N - \beta\phi'\right)}\right]^2}\right)d\phi' \tag{5a}$$

that is:

$$\begin{aligned} L = &\left[\frac{p}{2}\ln\left(1 + \frac{2p\beta}{\sqrt{p^2\beta^2 + a^2} - p\beta}\right) - \frac{1}{\beta}\sqrt{p^2\beta^2 + a^2}\right] \\ &- \left[\frac{p}{2}\ln\left(1 + \frac{2p\beta}{\sqrt{p^2\beta^2 + a^2\left(2\pi N\beta + 1\right)^2} - p\beta} - \frac{1}{\beta}\sqrt{p^2\beta^2 + a^2\left(2\pi N\beta + 1\right)^2}\right)\right] \end{aligned} \tag{5b}$$

and using the position vector $\bar{r}'$ of the log-helix as given in Eq. (1), it is a relatively simple matter to obtain the unit vector $\hat{a}_{\ell'}$ along the helical arm length as:

$$\hat{a}_{l'}=\frac{\dfrac{dr'}{d\phi'}}{\left|\dfrac{dr'}{d\phi'}\right|}=\frac{-\sin\phi'\hat{a}_x+\cos\phi'\hat{a}_y+\left[p\beta\Big/a\left(\Phi_N-\beta\phi'\right)\right]\hat{a}_z}{\sqrt{1+\left[p\beta\Big/a\left(\Phi_N-\beta\phi'\right)\right]^2}} \tag{6}$$

With these results, it is now a straightforward matter to specify the vector magnetic potential $\bar{A}$, due to an axially-directed distribution of current $\hat{a}_{\ell'}I(\ell')$ for the electrically thin-wire log-helix antenna as given by:

$$\bar{\mathrm{A}}=\frac{\mu_0}{4\pi}\int_{l'}\hat{a}_{l'}I\left(l'\right)\frac{e^{-jk_0R}}{R}dl' \tag{7}$$

where all symbols assume their usual definitions. Next, we invoke the conventional "magnitude and phase approximations" such that the quantity R appearing in the denominator of Eq. (7) is simply replaced by r the radial distance from the origin of spherical coordinate system to the field point, and the quantity R in the exponential term reduces to:

$$R\cong r-\hat{a}_r\cdot\bar{r}' \quad , \tag{8}$$

so that

$$R=r-a\sin\vartheta\cos\left(\phi-\phi'\right)-p\cos\vartheta\ln\left[\frac{\Phi_N}{\Phi_N-\beta\phi'}\right] \tag{8a}$$

A substitution of Eqs. (5), (6) and (8a) in Eq. (7) readily provides the following integral expressions for the ($A_x,\ A_y\ and\ A_z$) Cartesian components of the vector potential $\bar{A}$:

$$A_x=-\frac{\mu_0 ae^{-jk_0r}}{4\pi r}\int_0^{2\pi N}\sin\phi'I\left(\phi'\right)e^{jk_0\left[a\sin\vartheta\cos\left(\phi-\phi'\right)+p\cos\vartheta\ln\left(\frac{\Phi_N}{\Phi_N-\beta\phi'}\right)\right]}d\phi' \tag{9a}$$

$$A_y=\frac{\mu_0 ae^{-jk_0r}}{4\pi r}\int_0^{2\pi N}\cos\phi'I\left(\phi'\right)e^{jk_0\left[a\sin\vartheta\cos\left(\phi-\phi'\right)+p\cos\vartheta\ln\left(\frac{\Phi_N}{\Phi_N-\beta\phi'}\right)\right]}d\phi' \tag{9b}$$

$$A_z=\frac{\mu_0 p\beta e^{-jk_0r}}{4\pi r}\int_0^{2\pi N}\frac{1}{\Phi_N-\beta\phi'}I\left(\phi'\right)e^{jk_0\left[a\sin\vartheta\cos\left(\phi-\phi'\right)+p\cos\vartheta\ln\left(\frac{\Phi_N}{\Phi_N-\beta\phi'}\right)\right]}d\phi' \tag{9c}$$

In the far-zone of log-helix antenna, only two components of the electric field, namely $E_\theta\ and\ E_\phi$ are of practical interest, and are computable from:

$$\left.\begin{aligned}E_\vartheta&=-j\omega A_\vartheta\\E_\phi&=-j\omega A_\phi\end{aligned}\right\} \tag{10}$$

after the conversion of the rectangular components of $\bar{A}$ to the spherical components by the use of the usual coordinate transformation equations:

$$E_\vartheta=\frac{-j\omega\mu_0e^{-jk_0r}}{4\pi r}\int_0^{2\pi N}\left[a\cos\vartheta\sin\left(\phi-\phi'\right)-\frac{p\beta\sin\phi}{\Phi_N-\beta\phi'}\right]I\left(\phi'\right)e^{jk_0\left[a\sin\vartheta\cos\left(\phi-\phi'\right)+p\cos\vartheta\ln\left(\frac{\Phi_N}{\Phi_N-\beta\phi'}\right)\right]}d\phi' \tag{11a}$$

$$E_\phi=\frac{-j\omega\mu_0e^{-jk_0r}}{4\pi r}\int_0^{2\pi N}\left[\cos\left(\phi-\phi'\right)\right]I\left(\phi'\right)e^{jk_0\left[a\sin\vartheta\cos\left(\phi-\phi'\right)+p\cos\vartheta\ln\left(\frac{\Phi_N}{\Phi_N-\beta\phi'}\right)\right]}d\phi' \tag{11b}$$

The unknown distribution of current along the axis of the log-helix can now be determined using the method of moments in a manner comprehensively described in [19, 20], following which the antenna's input and far-zone characteristics can be obtained. For computational purposes, the axial ratio (AR) and the power gain (G_p) along the helical axis ($\theta = 0^o$, $\phi = 0^o$) are determined from the respective standard antenna parameter expressions:

$$AR(dB) = 10\log_{10}\left[\frac{|E_\vartheta|^2+|E_\phi|^2+\left[|E_\vartheta|^4+|E_\phi|^4+2|E_\vartheta|^2|E_\phi|^2\cos(2\delta)\right]^{1/2}}{|E_\vartheta|^2+|E_\phi|^2-\left[|E_\vartheta|^4+|E_\phi|^4+2|E_\vartheta|^2|E_\phi|^2\cos(2\delta)\right]^{1/2}}\right] \quad (12)$$

where δ denotes the time-phase difference between the field components [21], and

$$G_p(dBi) = 10\log_{10}\left[\frac{\left(|E_\vartheta|^2+|E_\phi|^2\right)r^2}{30|I_{in}|^2R_{in}}\right] \quad (13)$$

in which $|I_{in}|$ is the magnitude of antenna current at feed point, R_{in} stands for the corresponding input resistance of the antenna, and r is the radial distance from the coordinate origin to the far-field point [22].

3. DISCUSSION OF THE COMPUTATIONAL RESULTS

For the purposes of numerical computations, choice of antenna dimensions is informed by the fact - established by Kraus [23] - that for axial mode operations, normalized circumference (C_λ), pitch angle (α), and number of turns 'N' are respectively restricted according to $0.8 \le C_\lambda \le 1.2; 12° \le \alpha \le 14°; N \ge 4$. Consequently, a log-helix derived from an 8-turn uniform helix having a pitch angle of 13° and circumference of one wavelength (1λ) at a frequency of 2 GHz is selected as candidate example. The extent of departure from the uniform helix's profile increases as β increases as shown in the z′ curves of Fig. 2. In particular, the curvature of the log plots increases as β increases with the physical consequence that the consecutive turns at the upper end flares out while the turns at the lower end are in close proximity to each other. As a matter of fact, when β = 0.1, the span of the antenna's last two turns constitutes 45% of its total axial length, whereas the extent of the last two turns of the uniform helix take only 25% of the total axial length. On the other hand, the span of the first two turns of the log-helix accounts for 13% of the total axial length. This is unlike the case of the uniform helix, for which the corresponding span covers 25% of the entire axial length. At the lower value of β = 0.01, the first two turns take up 21% of the total axial length while the last two turns occupy 30% of the total volume associated with the log-helix. A simple inference from these observations is that as β increases, the open end of log-helix flares out whereas turns at the feed end are closer to each other. As a matter of fact, as the logarithmic variation factor increases, the antenna arm length gradually increases, so that keeping axial height constant results in the compression described in the foregoing. Further insight into the physical characteristics of log-helix is available from the profiles of Fig. 2(b), which describe how pitch angle varies with ϕ′ for different values of β ranging from 0.01 to 0.1.

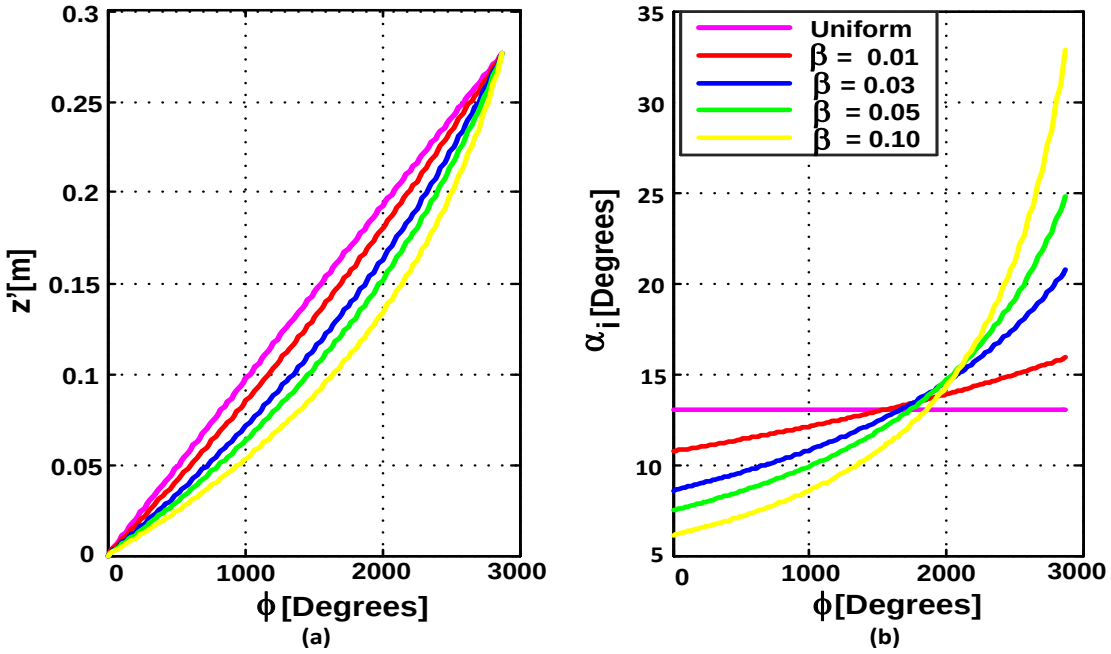

Fig. 2. Log-helix antenna geometry: a) axial profiles for different values of β; b) distribution of pitch angle α_i.

It is evident from the pitch angle profiles that the pitch angle, in general, increases along the log-helix structure. At the feed-end ($\phi° = 0$), the pitch angle decreases as β increases, and for all values of β, the pitch angle of the log-helix is lower than that of the uniform helix. Conversely, at the open-end ($\phi° = 2\pi N$), the pitch angle takes higher values as β increases, and is greater than that of the uniform helix for β values of interest in this paper. These physical characteristics are consistent with the characterizing profiles of the z′ plots discussed earlier. It is worth remarking that the pitch angle profile of log-helix has a continuously changing positive slope along its structure, which is different from that for the non-uniform helix of linearly varying pitch angle characterized by constant slope along its configuration [11]. It is also to be noted that as β decreases, the profile approaches that of a uniform helix, and in the limit, as $\beta \to 0$, it is seen from Eqs. (3) and (4a) (through an application of L'Hospital rule) that the particular case of the uniform-spacing helix is obtained. When in addition 'α' is set to 0 and N=1, the geometry of a circular loop of radius 'a' located on the X-Y plane is prescribed.

3.1. Current Distributions

In order to examine the influence of parameter β on the log-helix's current distributions, current profiles for values of β ranging between 0.01 and 0.1 are superimposed on the same plots together with the current distribution on the corresponding uniform helix, when the circumference in wavelengths (C_λ) ranges between 0.8 and 1.3 at the operating frequency of 2 GHz. Fig. 3(a) displays the current distribution profiles for the log-helix and uniform helix antennas when C_λ varies from 0.8 to 0.95 and β lies between 0.01 and 0.1. For the case C_λ = 0.8, the current profiles consist of two distinct parts, namely exponentially decaying component existing approximately over seventy percent of the log-helix structure from the feed-end; and a surface wave component of extremely small magnitude, extending over the remaining thirty percent. With a slight increase of C_λ to 0.85, the exponential

component of the current distribution becomes limited in extent (to the first three turns of the helix) while the surface wave segment extends over the last five turns, even though with some visible ripples due to reflections from the open end. It can be seen that for the cases C_λ = 0.90 and 0.95, the surface wave part of the current distribution - which has been established [3] as the main contributor to the radiation in the axial direction - is now well developed starting from the third turn of the helix to the end whilst the exponential component is restricted to the first two turns of the helix. It is observed that the magnitude of current for the log-helix increases with C_λ as β increases, and is larger - in all cases - than that for corresponding uniform helix.

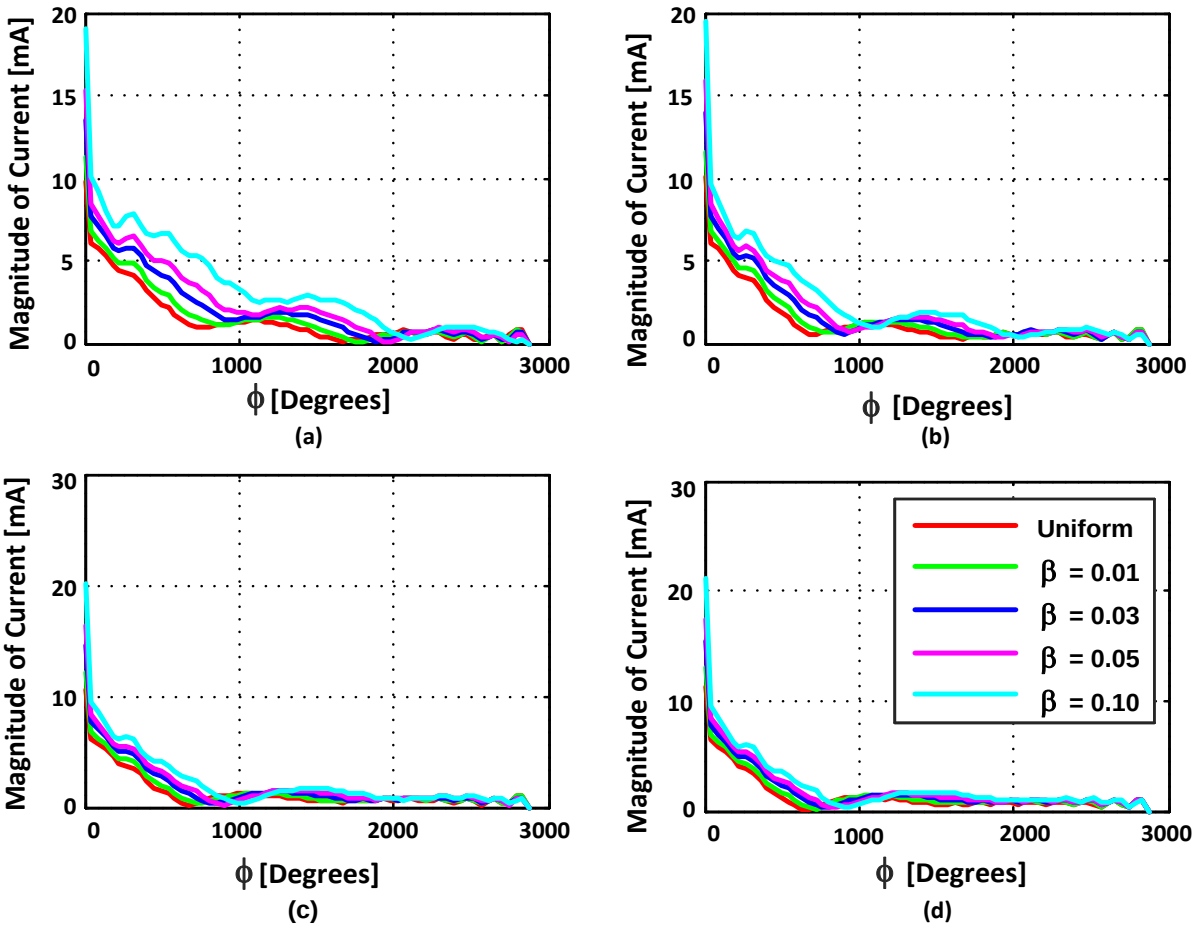

Fig. 3. Current distribution profiles along the log-helix and uniform helix for 0.80 ≤ C_λ ≤ 0.95: a) C_λ = 0.80; b) C_λ = 0.85; c) C_λ = 0.90; d) C_λ = 0.95.

In the case of Fig. 4 - which displays the distributions of current when C_λ assumes values between 1.00 and 1.15 - it is seen that there are significant improvements in the surface wave components in terms of higher magnitudes, smoothness and extent over the antenna axis. The distinction between the surface wave components for different values of β is not readily apparent whereas the exponential wave parts are well defined for each value of β and extend between the feed-point and the first 1½ turns of the helix. As earlier observed for Fig. 3, the current magnitudes for 0.9 ≤ C_λ ≤ 1.15 steadily increase as β increases, and for all the examined cases, the current magnitude of the uniform helix is smallest.

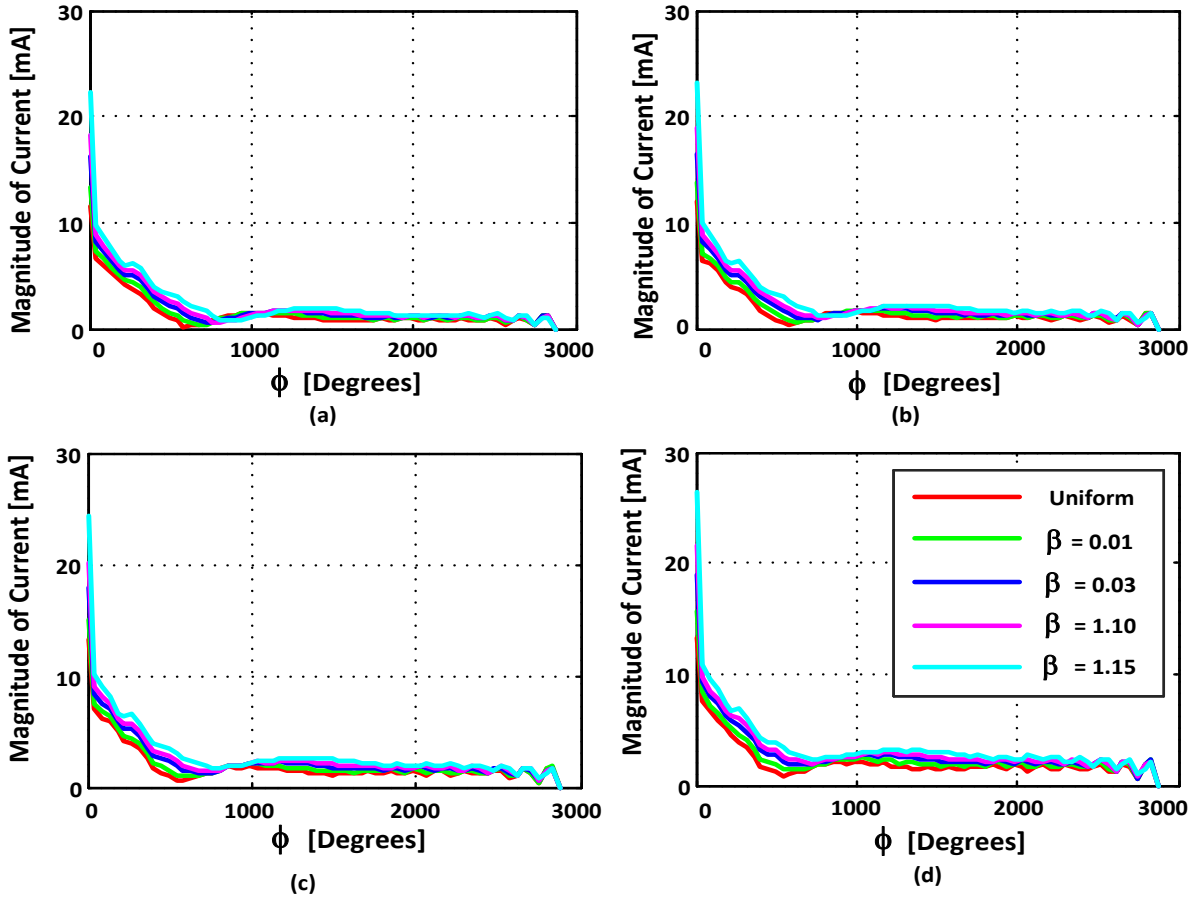

Fig. 4. Current distribution profiles of log-helix and uniform helix for $1.00 \leq C_\lambda \leq 1.15$: a) $C_\lambda = 1.00$; b) $C_\lambda = 1.05$; c) $C_\lambda = 1.10$; d) $C_\lambda = 1.15$.

The current distribution profiles for C_λ taking on the values of 1.20, 1.25 and 1.30 are displayed in Fig. 5. They clearly show that the transition between the exponential and surface wave regions of the current distribution is not as sharply defined as obtained with lower values of C_λ. It can also be seen from Fig. 5 that the ripples on the surface wave components are now increasingly more prominent as β increases. Furthermore, the magnitude of current at the feed-point has increased significantly and the exponential part of the current reaches its minimum value within the first two turns of the log-helix.

For all the considered values of β, the magnitude of current for the uniform helix is lower than that of the log-helix. In order to examine the effects of turns proximity on the current behavior at the feed-point, the feed-point currents of uniform helix and log-helix as a function C_λ are plotted and discussed under the section on input characteristics of log-helix.

Current distribution profiles corresponding to different fixed values of the logarithmic variation factor, β, are displayed in Fig. 6. The profiles show that as β increases, the starting point of the surface wave section moves towards the third turn of the log-helix, with corresponding increase in magnitude. It is also to be noted that the ripples in the surface wave region become markedly visible for values of C_λ greater than 1.00 as β assumes higher values. And that for all values of β, the transition from the exponential decaying part to the surface wave portion is sufficiently smooth for the two cases $C_\lambda = 0.90$ and 1.00; but not too distinct for $C_\lambda = 1.20$, 1.25 and 1.30.

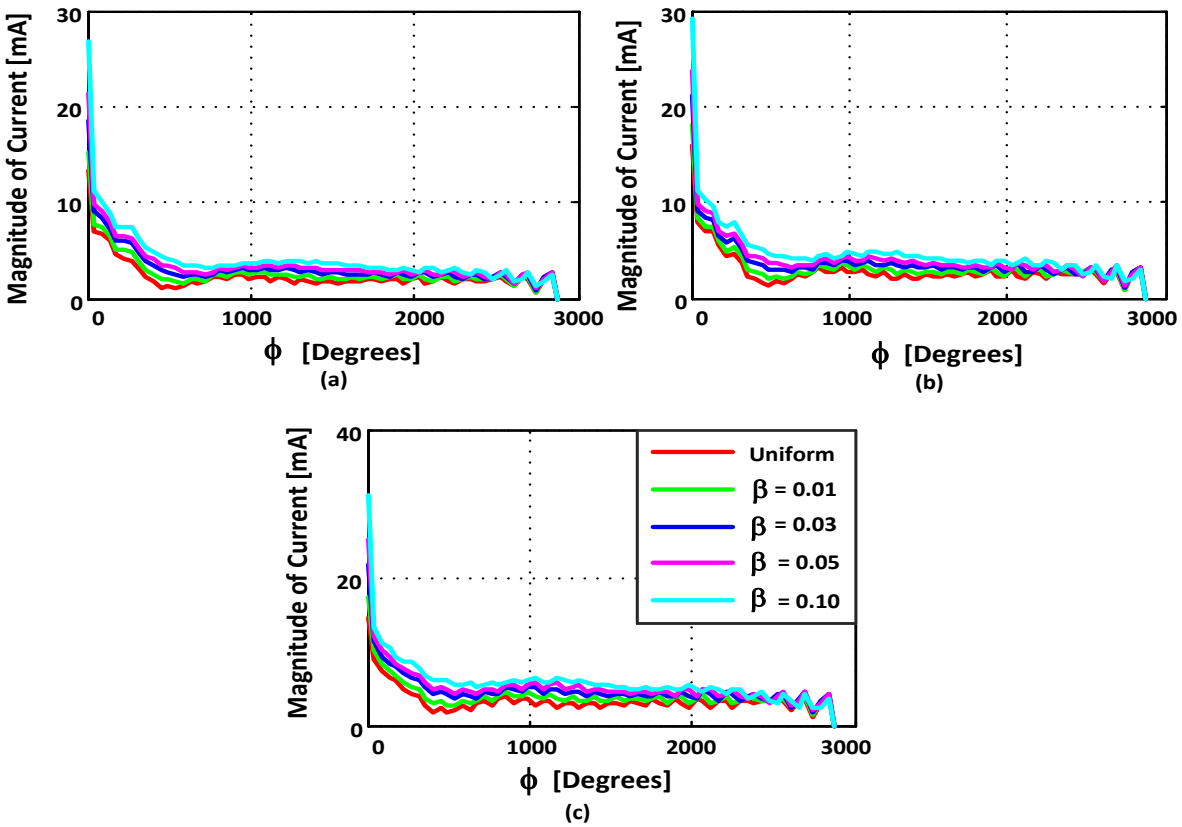

Fig. 5. Axially-directed current distributions for the log- and uniform helix antennas for $1.20 \leq C_\lambda \leq 1.30$: a) $C_\lambda = 1.20$; b) $C_\lambda = 1.25$; c) $C_\lambda = 1.30$.

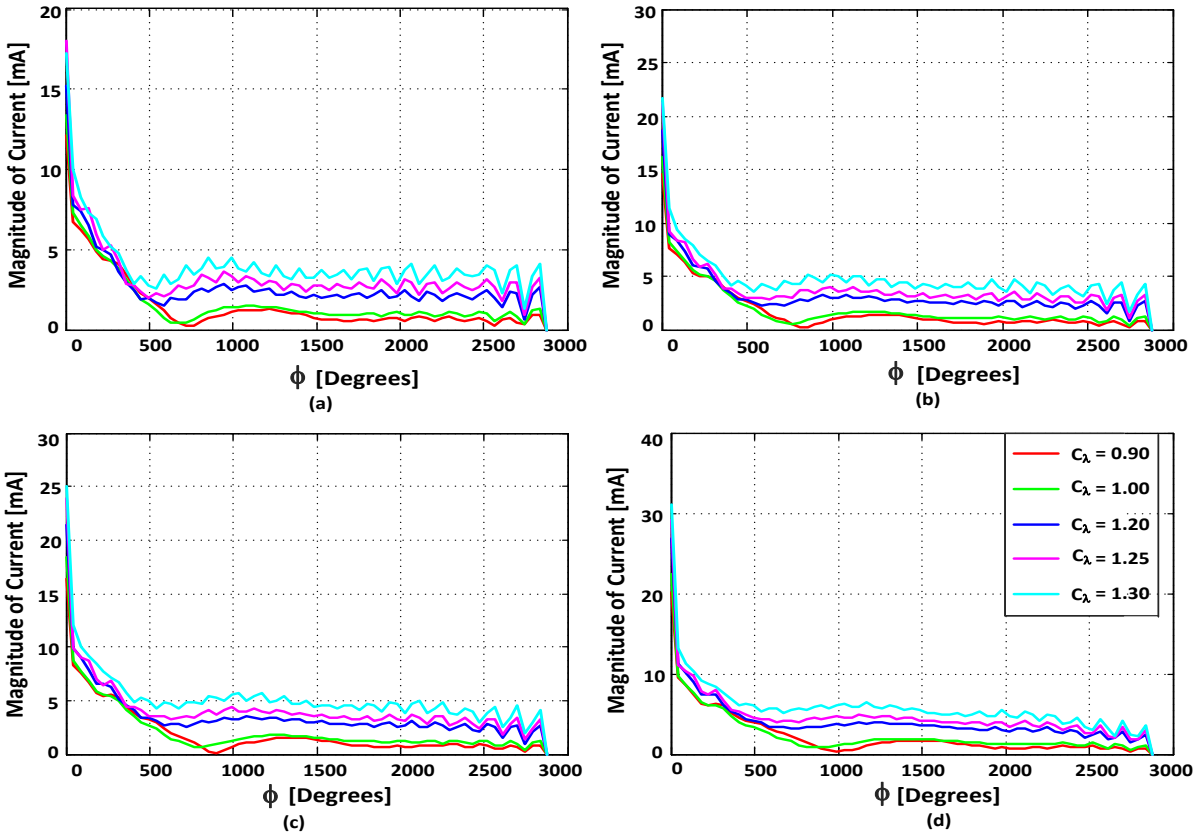

Fig. 6. Current distributions along the axis of the log-helix for fixed values of β, as C_λ varies : a) β = 0.01; b) β = 0.03; c) β= 0.05; d) β = 0.10.

3.2. Radiation-Zone Electric Fields

The illustrations of Figs. 7 to 14 describe the radiation-zone normalized electric field intensity patterns E_θ and E_ϕ on the $\phi = 0^o$ plane, for the log-helix and corresponding uniform helix. Figs. 7 to 9 display E_θ patterns for each value of C_λ considered, with the logarithmic variation factor β ranging between 0.01 and 0.10. For values of C_λ lying between 0.80 and 0.95, Fig. 7(a) shows that although the normalized radiated beam patterns are sharper with decreasing values of β, the corresponding minor lobes become significantly more pronounced so that the beam directivity (as shown by computational data) of E_ϑ patterns improves as β increases. It can also be seen that the pattern sidelobes are most prominent for the uniform helix. Furthermore, it is readily observed that the main beams of E_θ patterns are well-aligned along the helical axis and fully symmetrical about the axis of the helical structure. In all situations, there is null radiation in the lower space of the antenna configuration as a consequence of the infinite size of the supporting ground plane.

Patterns in Fig. 8 are for the cases of C_λ values from 1.00 to 1.15, and reveal that the main beams of the E_θ patterns are essentially identical without significant sidelobes for all values of β considered. However, the E_θ patterns of the uniform helix are typified by sizeable sidelobes when compared with the corresponding sidelobes for the log-helix antenna patterns. Furthermore, the patterns become more directive as C_λ increases with associated reduction in the half-power beamwidth of the major lobes. This is evident from the numerical values of power gain - displayed in Table 1 - for different values of C_λ and β. It is also to be observed from Fig. 8 that the symmetry of the main lobes about the helical axis is preserved, while the development of the sidelobes as C_λ increases is very moderate. For C_λ that equals 1.15 and $\beta = 0.1$, the sidelobes have been fully developed, though less than 20% of the main lobe level.

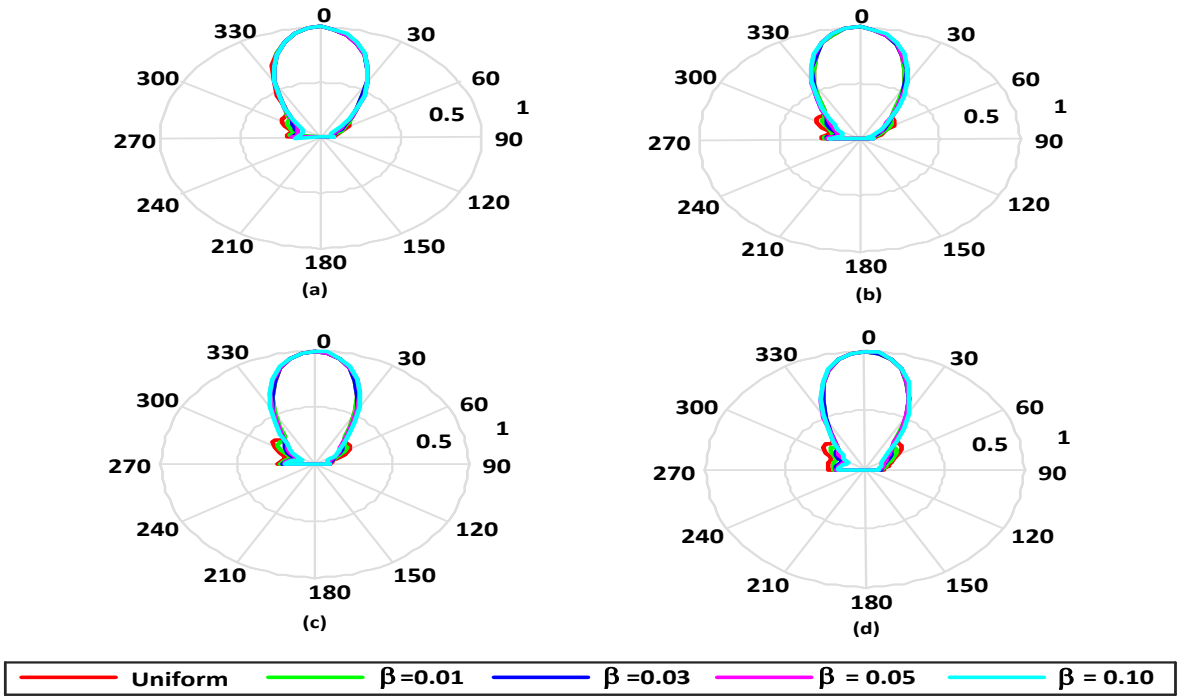

Fig. 7. $E_\vartheta(\vartheta, 0°)$ components of the normalized radiated electric fields of the log-helix and uniform helix for $0.80 \le C_\lambda \le 0.95$: a) $C_\lambda = 0.80$; b) $C_\lambda = 0.85$; c) $C_\lambda = 0.90$; d) $C_\lambda = 0.95$.

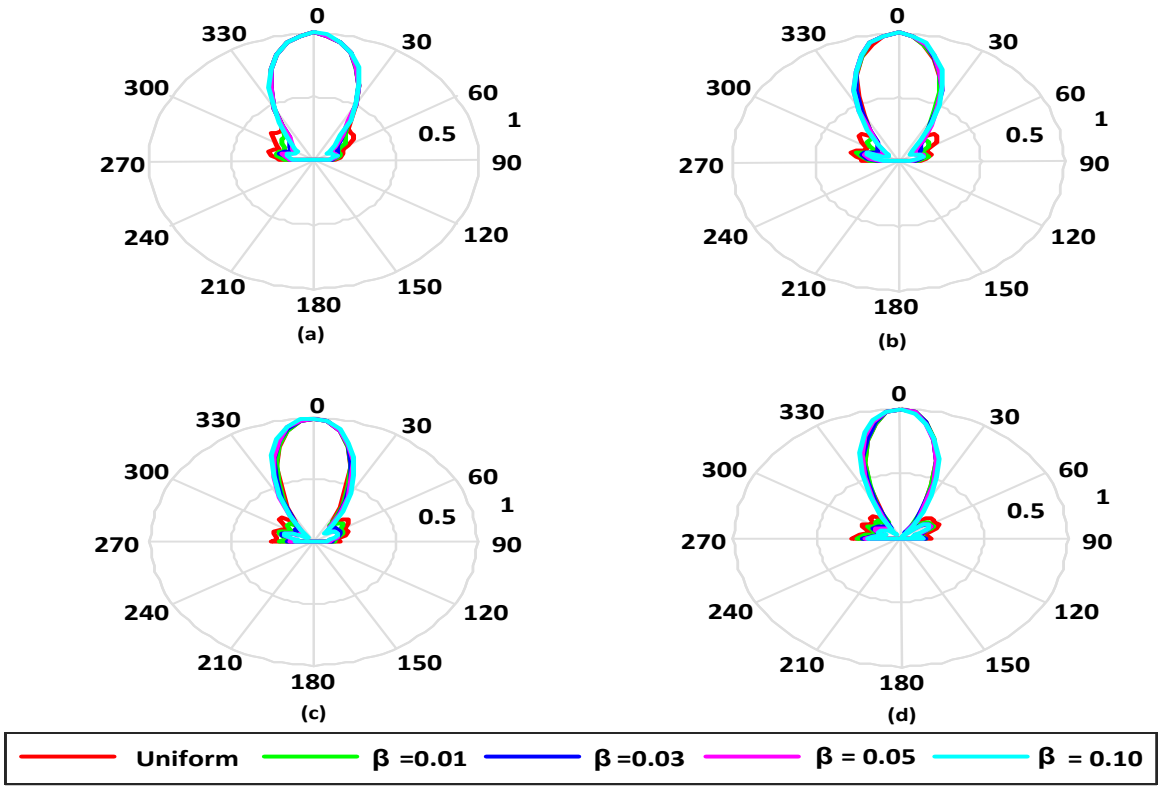

Fig. 8. $E_{\vartheta}(\vartheta, 0°)$ components of the normalized radiated electric fields of the log-helix and uniform helix for $1.00 \leq C_{\lambda} \leq 1.15$: a) $C_{\lambda} = 1.00$; b) $C_{\lambda} = 1.05$; c) $C_{\lambda} = 1.10$; d) $C_{\lambda} = 1.15$.

Table 1. Variation of power gain with normalized circumference for different values of β.

	Power gain [dB]				
C_{λ}	Uniform	β =0.01	β = 0.03	β=0.05	β=0.1
0.80	4.288	4.749	5.08	5.141	4.929
0.85	5.438	6.108	6.736	7.043	7.395
0.90	6.434	7.235	8.016	8.425	8.953
0.95	7.408	8.275	9.124	9.574	10.166
1.00	8.354	9.281	10.16	10.614	11.203
1.05	9.182	10.165	11.076	11.531	12.091
1.10	9.964	10.935	11.825	12.259	12.768
1.15	10.781	11.742	12.539	12.888	13.252
1.20	11.235	12.298	13.097	13.378	13.55
1.25	11.25	12.294	13.054	13.258	13.218
1.30	11.377	12.373	12.866	12.827	12.305

Again, as a consequence of the infinite extent of the ground plane featuring in the feeding arrangement, there is null radiation into the lower space ($z < 0$) of the antenna system. The corresponding E_{θ} patterns for C_{λ} equals 1.20, 1.25 and 1.30 and the selected values of β from 0.01 to 0.10 are depicted in Fig. 9. Though the directivity of the main beams has been enhanced considerably at high values of C_{λ}, the formation and levels of the undesirable sidelobes of the patterns are now significant. As remarked for previous cases, the E_{θ} patterns of log-helix are better than those of the uniform helix. For all the values of β considered, the main lobes of the E_{θ} patterns remain essentially the same irrespective of the

values of C_λ. In sum, Figs. 7 to 9 have clearly shown that the log-helix radiates satisfactorily in the axial-mode when moderate values are prescribed for the parameter β. Further insights into the axial-mode radiation performance of the log-helix using antenna metrics such as axial ratio and power gain will be presented in another section.

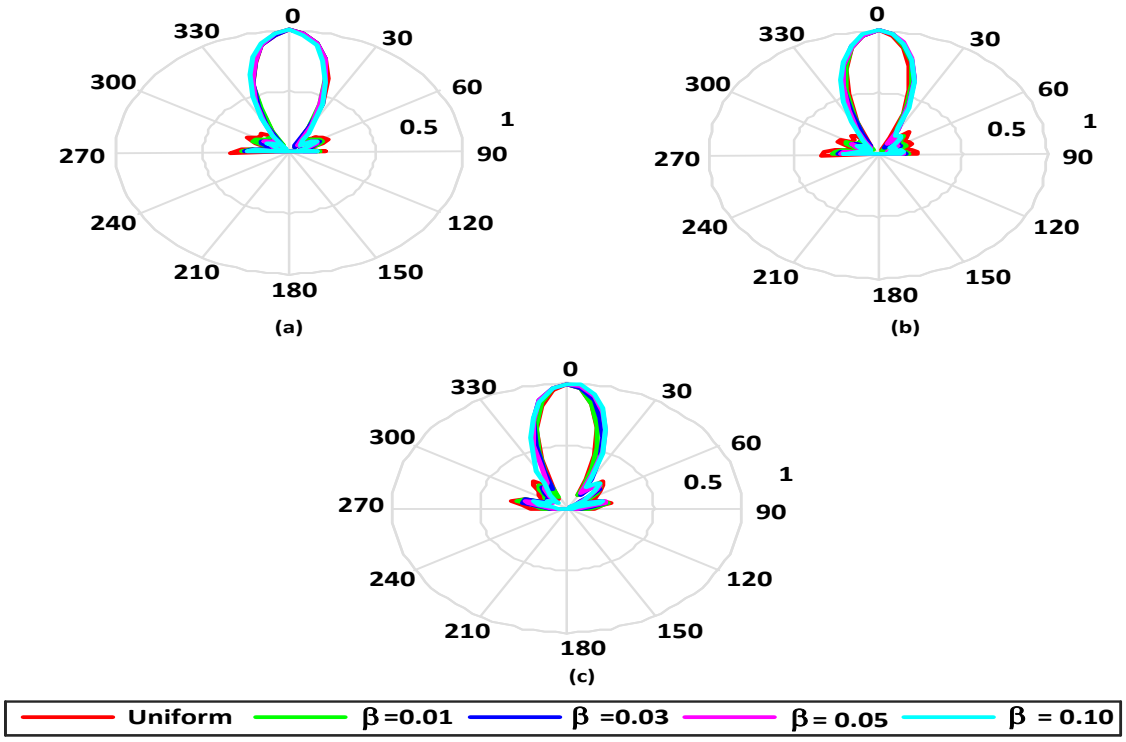

Fig. 9. $E_\vartheta(\vartheta, 0°)$ components of the normalized radiated electric fields of the log-helix and uniform helix for $1.20 \leq C_\lambda \leq 1.30$: a) $C_\lambda = 1.20$; b) $C_\lambda = 1.25$; c) $C_\lambda = 1.30$.

Fig. 10 displays the E_θ patterns of the log-helix when β is fixed and the helix circumference in wavelengths (C_λ) is varied from 0.80 to 1.30. It is noted that regardless of the values of β and C_λ, the log-helix radiates maximally in the axial direction with some associated minor lobes off the helix axis. As expected, the E_θ patterns for $C_\lambda = 1.30$ are the most directive but characterized by significant sidelobes. The radiation performance of the log-helix appears to be most attractive at $C_\lambda = 1.00$, which may be classified as the optimum log-helix electrical circumference, synonymous with the well-established value for the uniform helix.

The normalized E_ϕ patterns of the log-helix as well as those of the corresponding uniform helix on the $\phi = 0^o$ plane are plotted and presented in Figs. 11 to 13 when C_λ varies from 0.80 to 1.30 and β assumes values between 0.01 and 0.10. From the aforementioned figures, it is evident that the main lobes of the E_ϕ patterns are symmetrical about the helix axis and become more directive as C_λ attains higher values. As usual, the enhancement in the main lobes is traded off by the increase in the sidelobe size and the level of the E_ϕ patterns, especially when C_λ is greater than 1.15. In all scenarios here, the log-helix antenna is characterized by better E_ϕ patterns in comparison with those of the uniform helix. As highlighted for the E_θ patterns, there is zero radiation in the lower space ($z < 0$) of the antenna configuration as a result of the infinite extent of the ground plane counterpoise

deployed in the antenna feeding scheme. Perhaps, the enhanced sidelobes of the E_ϕ patterns when C_λ is greater than 1.15 may be attributed to the strong reflections of the current from the open end of the log-helix as underscored by noticeable ripples on the associated current waveforms.

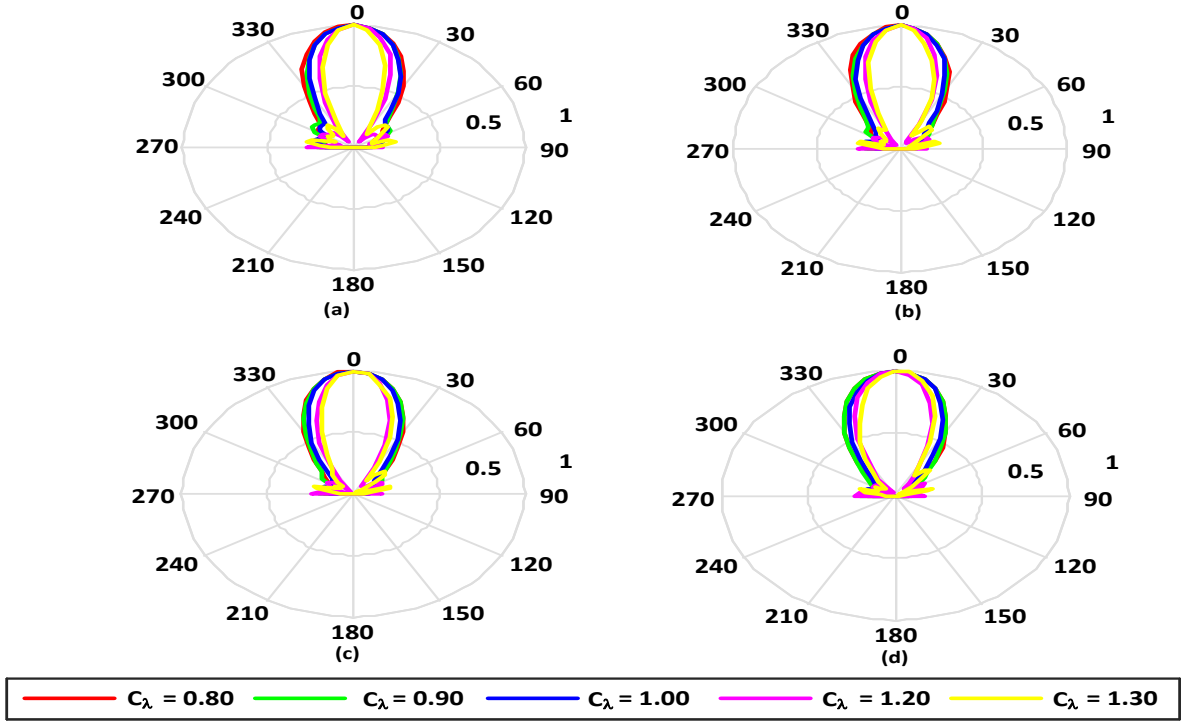

Fig. 10. Profiles, for various values of C_λ, of $E_\vartheta(\vartheta, 0°)$ components of the normalized radiated electric fields of the log-helix and uniform helix for fixed values of β: a) β = 0.01; b) β = 0.03; c) β= 0.05; d) β = 0.10.

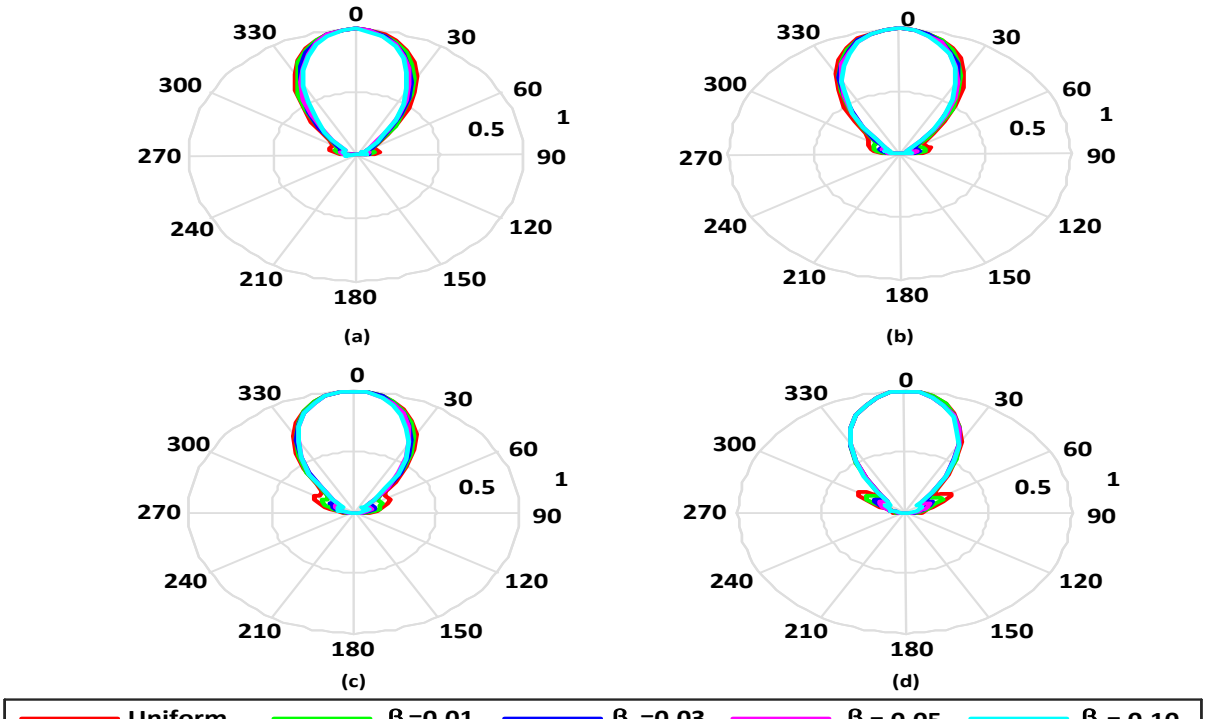

Fig. 11. $E_\phi(\vartheta, 0°)$ components of the normalized radiated electric fields of the log-helix and uniform helix for $0.80 \le C_\lambda \le 0.95$: a) C_λ = 0.80; b) C_λ = 0.85; c) C_λ = 0.90; d) C_λ = 0.95.

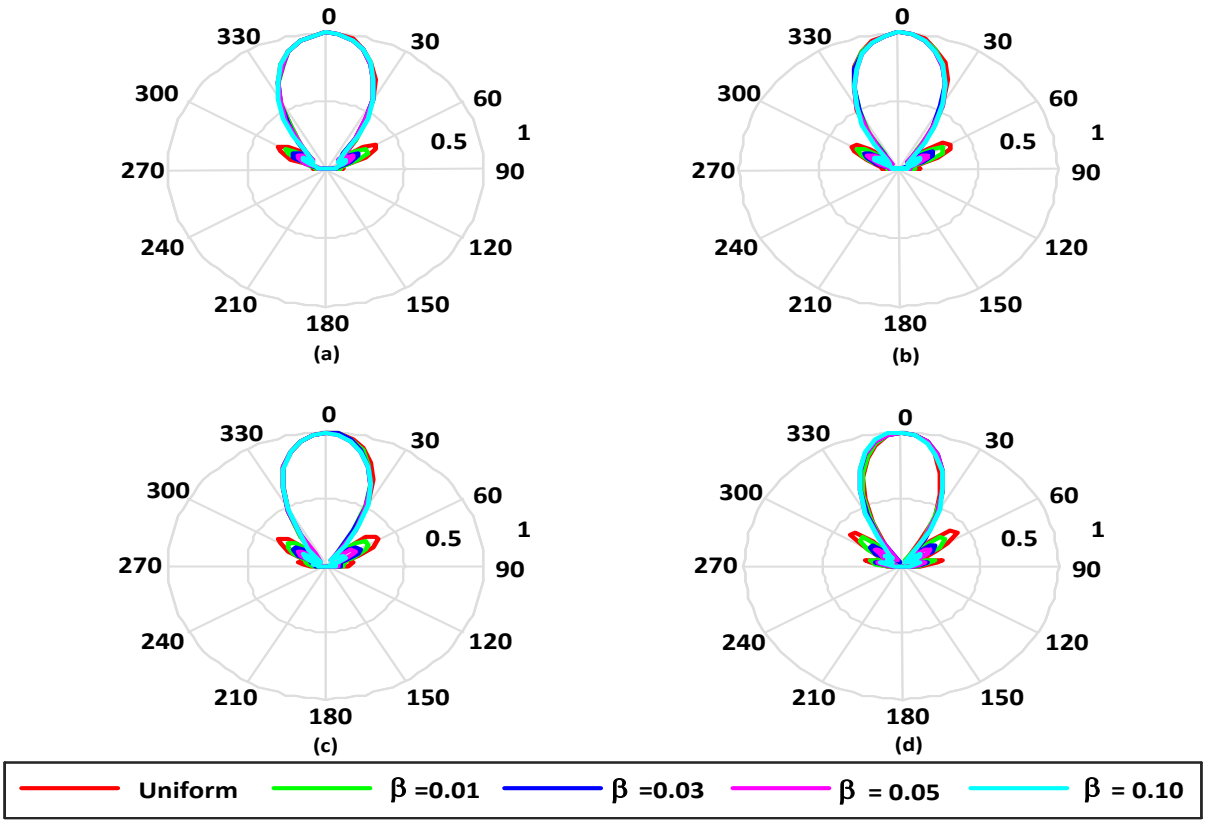

Fig. 12. $E_\phi(\vartheta, 0°)$ components of the normalized radiated electric fields of the log-helix and uniform helix for $1.00 \leq C_\lambda \leq 1.15$: a) $C_\lambda = 1.00$; b) $C_\lambda = 1.05$; c) $C_\lambda = 1.10$; d) $C_\lambda = 1.15$.

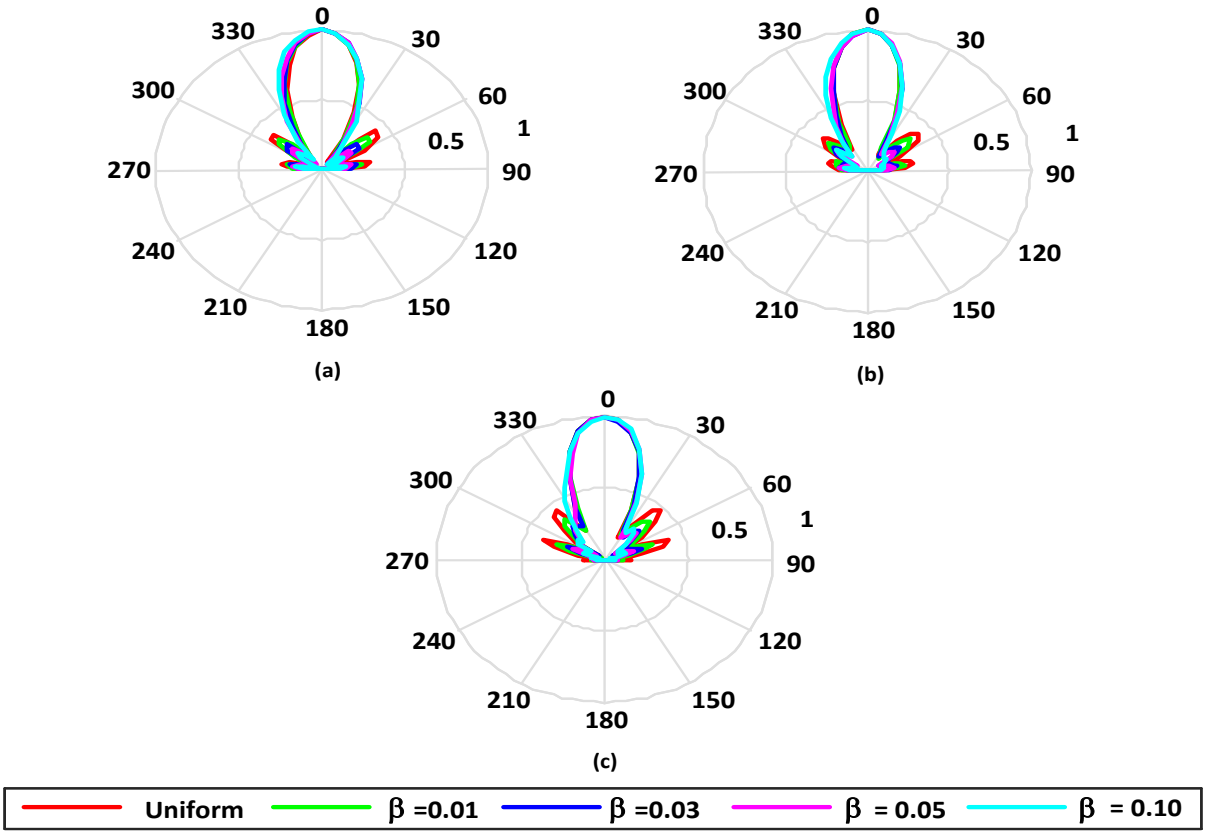

Fig. 13. $E_\phi(\vartheta, 0°)$ components of the normalized radiated electric fields of the log-helix and uniform helix for $1.20 \leq C_\lambda \leq 1.30$: a) $C_\lambda = 1.20$; b) $C_\lambda = 1.25$; c) $C_\lambda = 1.30$.

Finally, the E_ϕ patterns when β is fixed and C_λ is allowed to assume different values are portrayed in Fig. 14. It is apparent that for each value of β, the directivity of the E_ϕ patterns increases as C_λ increases, but with corresponding increase in the sidelobe levels. A careful inspection of the E_ϕ patterns shows that for β = 0.05, the E_ϕ patterns for all C_λ considered are the most attractive. It is also observed that the symmetry of the E_ϕ patterns about the helix axis is maintained in all cases of interest here.

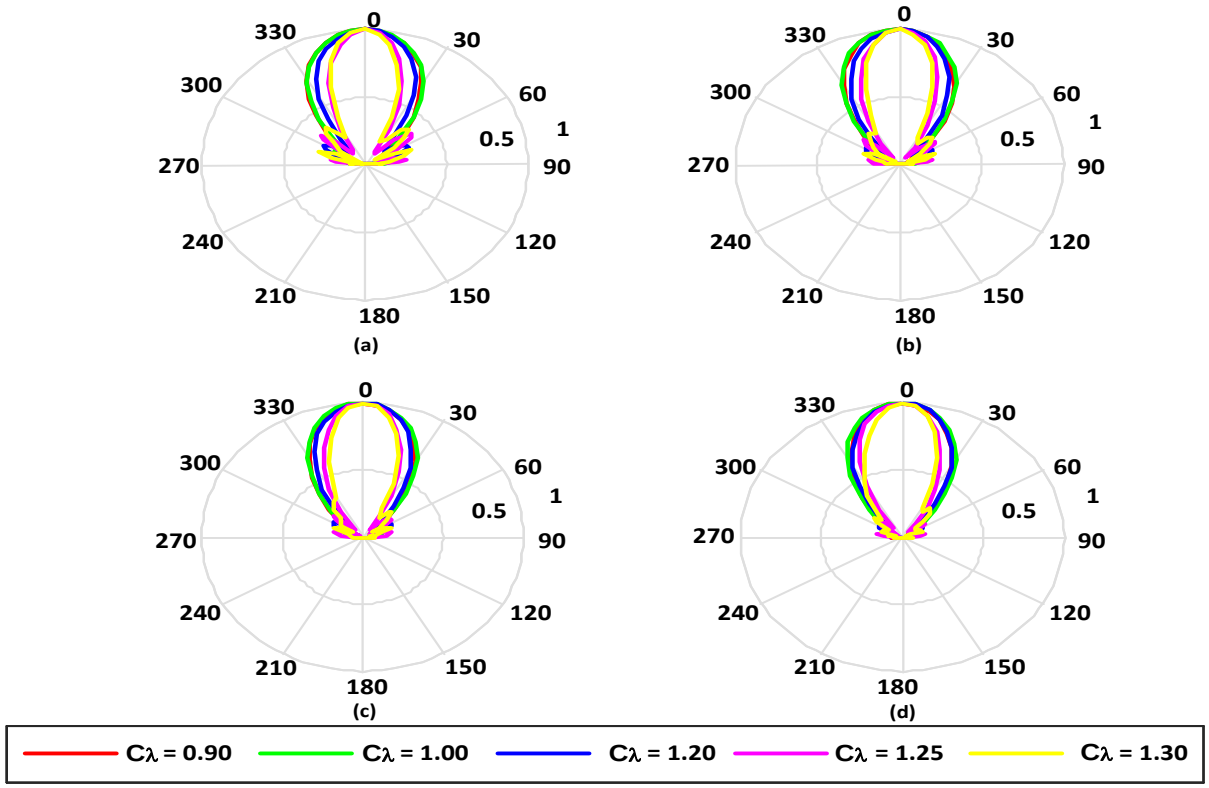

Fig. 14. Profiles, for various values of C_λ, of normalized $E_\phi(\vartheta, 0°)$ components of the radiated electric fields of the log-helix and uniform helix for fixed values of β: a) β = 0.01; b) β = 0.03; c) β= 0.05; d) β = 0.10.

3.3. Input Characteristics: Feed-Point Current and Input Impedance

Towards further elucidation of the influence of logarithmic profile of the log-helix structure on its input characteristics, features of computational results for the magnitude of current at feed-point and the input impedance for various values of parameter β and helix circumference in wavelengths (C_λ) are displayed in Fig. 15. Profiles – exhibited in Fig. 15(a) - describe the variations of the magnitude of current at feed-point for specific values of β when C_λ lies in the range from 0.8 to 1.3 for the log-helix, as well as for the uniform helix for ease of comparison. It is evident from the profiles that for all values of β (0.01 – 0.10), feed-point current of the log-helix is of higher magnitude compared to that of the uniform helix, and there is progressive increase in the feed-point current as β increases. The profiles of feed-point current versus C_λ appear somewhat linear until C_λ is greater than 1.2, and a percentage increase of more than 50% is observed in the feed-point current magnitude when β changes from 0.01 to 0.10. It may, therefore, be inferred that the log-helix draws more current than the uniform helix from an identical feeding system.

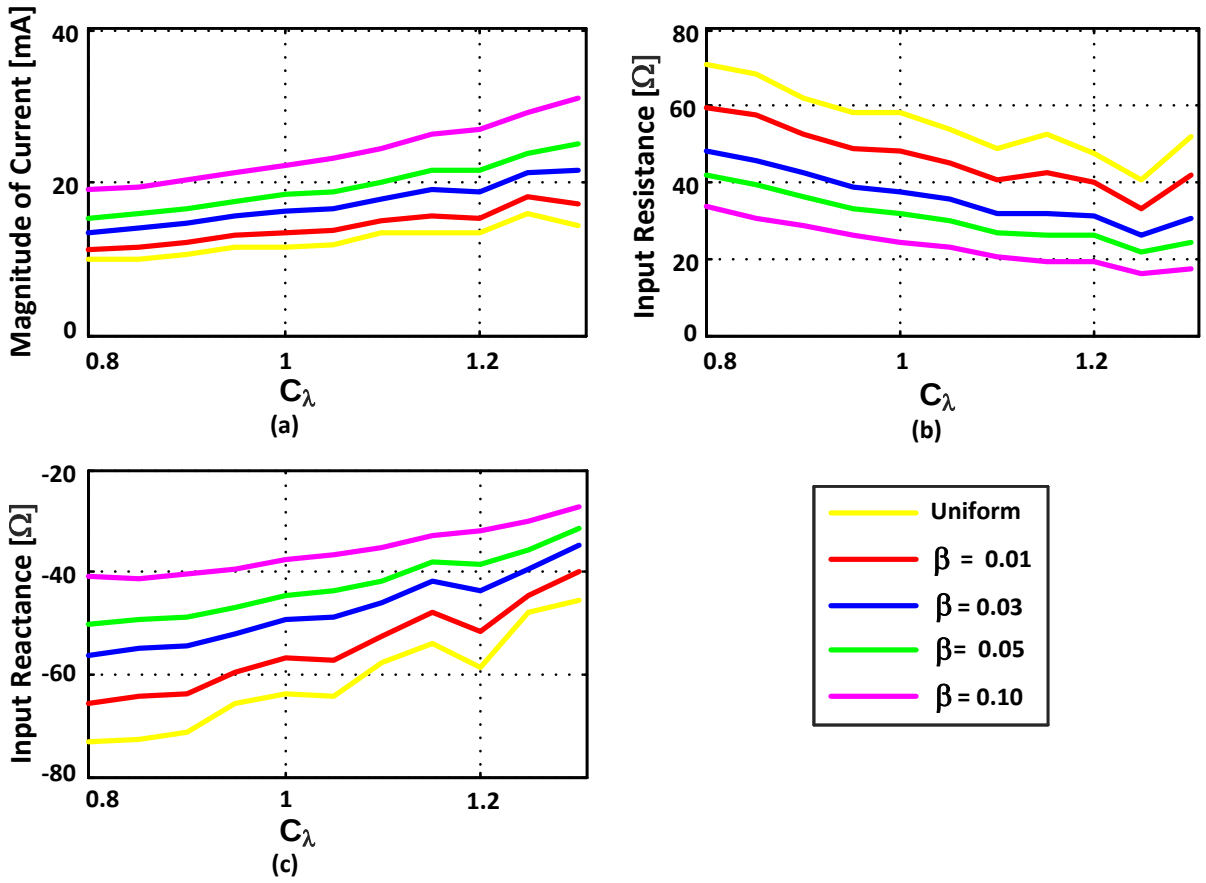

Fig. 15. Log-helix input characteristics: a) feed-point for $0.01 \le \beta \le 0.1$; b) profiles of input resistance R_{in} for $0.01 \le \beta \le 0.1$; c) input reactance (X_{in}) profiles for $0.01 \le \beta \le 0.1$.

The resistive part of the input impedance is illustrated in Fig. 15(b) for the values of β and C_λ of interest in this paper. The profiles show that the input resistance (R_{in}) at the feed point decreases as C_λ increases. For the different values of β and C_λ utilized, R_{in} for the uniform helix is greater than corresponding values for the log-helix. Remarkably, the input resistance of the log-helix varies reasonably between 20 Ω and 60 Ω, slopes downwards gradually as C_λ increases for all values of β.

Fig. 15(c) depicts the input reactance (X_{in}) of the log-helix as well as that of the uniform helix for values of β and C_λ considered in this paper. The input reactance is entirely capacitive as a result of the analytical model adopted for the feeding scheme. The X_{in} of the uniform helix assumes higher values vis-a-vis those of the log-helix, which lie between - 40 Ω and - 65 Ω. A merit of the moderate variation of the input reactance is the ease of designing a matching network since the reactance of the log-helix decreases as C_λ increases irrespective of the value of β.

3.4. Far-Zone Characteristics: Axial Ratio and Power Gain

The axial ratio (AR) profiles, due to computational results compiled with Eq. (12), and presented in Fig. 16(a) clearly show that the AR is essentially less than 3 dB for all values of β and C_λ considered in this paper. Thus, on the basis of usual 3 dB axial ratio criterion, the log-helix antenna radiates electromagnetic fields, characterized by acceptable degrees of circular

polarization, and may be classified as a circularly polarized antenna. It should be remarked that when C_λ lies between 0.90 and 1.10, the log-helix of β, equal to 0.01 has better AR than other log-helix antennas whose β is greater than 0.01. Specifically, Table 2 displays the values of axial ratio for different values of C_λ and β.

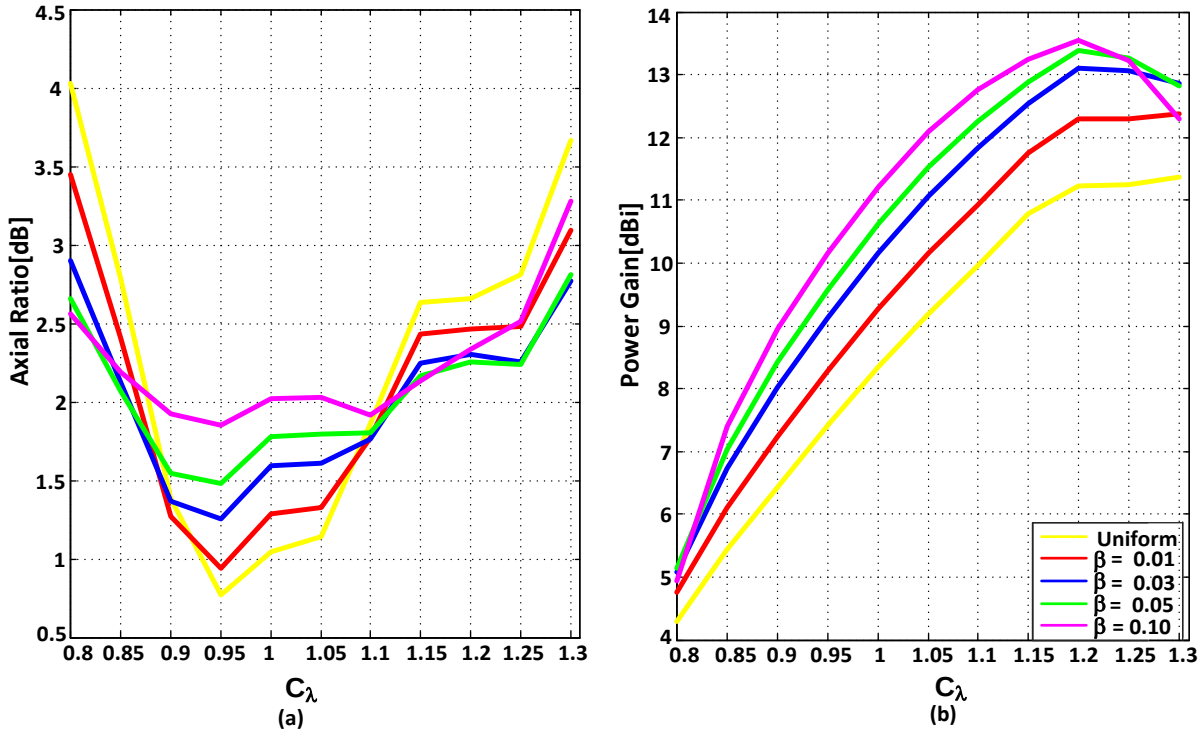

Fig. 16. Axial ratio and power gain performance: a) axial ratio for 0.01 ≤ β ≤ 0.1; b) profiles of power gain for 0.01 ≤ β ≤ 0.1.

Table 2: Axial ratio with normalized circumference for different values of β.

Axial Ratio [dB]					
C_λ	Uniform	β =0.01	β = 0.03	β=0.05	β=0.1
0.80	4.03	3.445	2.898	2.654	2.562
0.85	2.784	2.408	2.126	2.068	2.186
0.90	1.385	1.27	1.366	1.545	1.922
0.95	0.772	0.942	1.253	1.482	1.851
1.00	1.044	1.284	1.592	1.778	2.02
1.05	1.138	1.329	1.61	1.791	2.03
1.10	1.856	1.768	1.76	1.803	1.912
1.15	2.636	2.431	2.245	2.165	2.13
1.20	2.654	2.461	2.303	2.257	2.337
1.25	2.813	2.477	2.251	2.239	2.512
1.30	3.665	3.095	2.769	2.808	3.281

One important conclusion arising from Table 2 and Fig. 16(a) is that for $0.9 \leq C_\lambda \leq 1.1$, axial ratio improves with decreasing values of β. On the other hand, axial ratio bandwidth actually increases with increasing values of β for the 8-turn configuration under discussion.

Fig. 16(b) displays the plots of the power gain against C_λ for various values of β in addition to the plot for the uniform helix. It is seen from the power gain behaviors that regardless of the values of β and C_λ, the log-helix outperforms the uniform helix. And the power gain of the log-helix increases somewhat linearly as C_λ increases and as β also increases. It may be deduced that the log-helix has better directivity than the uniform helix. Values of power gain for different values of C_λ and β, listed in Table 1, show that with the exceptions of $C_\lambda = 0.80;\ 0.85\ and\ 1.25$, the power gain generally increases with β. For these three cases, the values of gain for $\beta = 0.10$ are lower than for $\beta = 0.05$. This shows that for these cases, gain peaks at a lower frequency for $\beta = 0.10$ than for $\beta = 0.05$.

4. A COMPARATIVE PERFORMANCE EVALUATION

The performance evaluation, described in this section, compares the log-helix as prescribed by:

$$z = p \ln\left(\frac{\Phi_N}{\Phi_N - \beta\phi'}\right), \tag{14a}$$

and the exponential helix, with axial profile characterized by [7]:

$$z = S\left(e^{\phi'/C} - 1\right). \tag{14b}$$

For the particular case of C = 12, S = (17.6), p = {56}, and $\beta = 1/3$ concerning the 4-turn helical antenna treated in [7], the axial profiles of the exponential-spacing and logarithmic-spacing helices are almost identical; though their corresponding pitch angle profiles differ significantly for values of ϕ' greater than 700^o, as can be seen from Figs. 17(a) and 17(b). For computational purposes, the finite ground plane is modeled by a wire-grid in the manner described in [2]. The profiles of Figs. 17(c) and 17(d) compare axial ratio and power gain variations with frequency, respectively. It is readily observed from Fig. 17(c) that whereas axial ratio values for the two helical antennas are generally comparable, the axial ratio bandwidth for the log-helix (80.7%) is greater than that for the exponential helix (77.18%), in this representative case. It may be remarked that this trend features for all values of C and β, and for $\frac{1}{C} = 0.05$. Indeed, computational results reveal that when $\frac{1}{C} = 0.10$ the exponential helix, (unlike the log-helix for which $\beta = 0.10$) loses its axial-mode property.

The power gain variations with frequency for the particular case under discussion are displayed in Fig. 17(d). These profiles reveal that whereas power gains for the two non-uniform helical antenna types are - in general - comparable, values recorded by the exponential-helix are - in general - higher than those for the log-helix. Nonetheless, peak power gain for the log helix (12.93 dBi at about 1.9 GHz) is higher than that for the exponential helix, which is 12.89 dBi at 2 GHz.

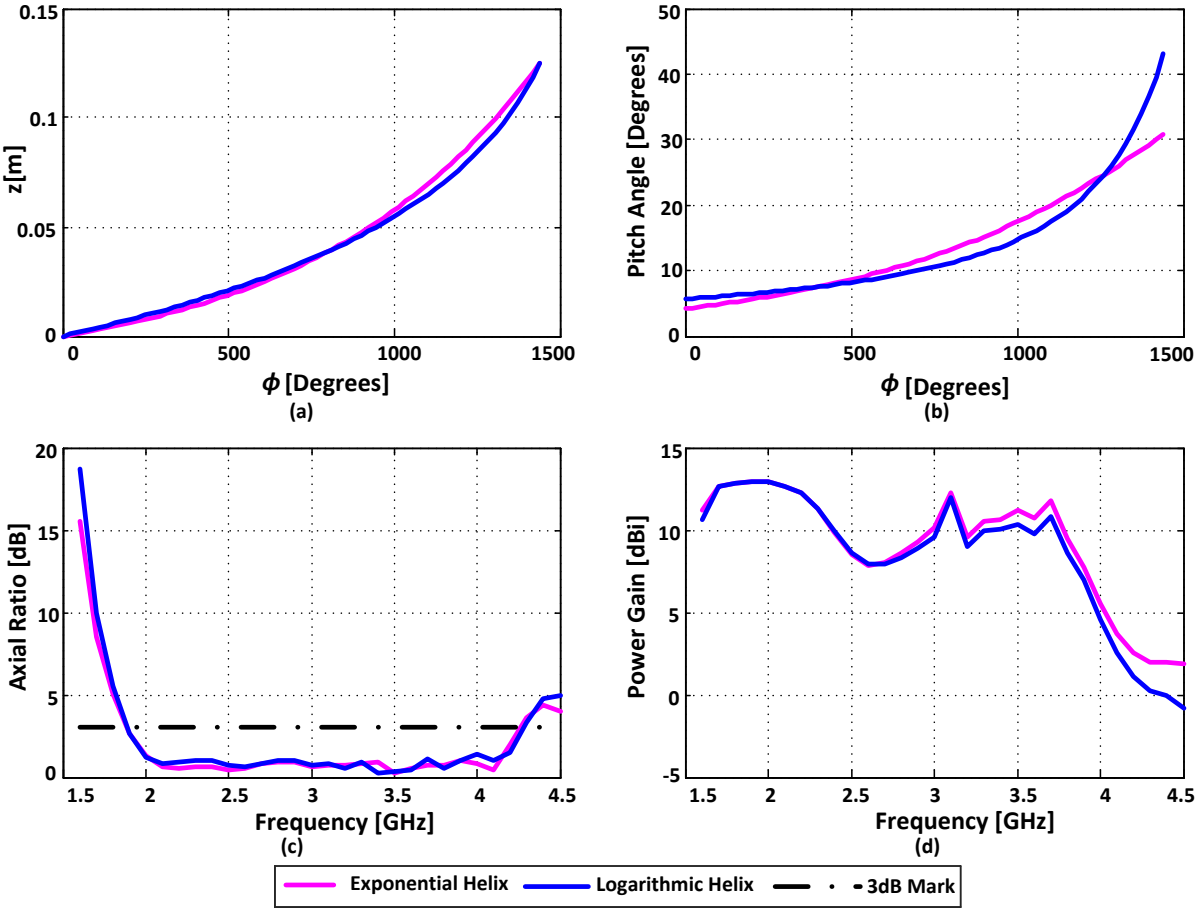

Fig. 17. Performance comparison of logarithmically-spaced and exponentially-spaced 4-turn non-uniform helical antennas: a) axial geometry profiles; b) pitch angle profiles; c) axial-ratio profiles; d) power-gain profiles.

5. CONCLUSIONS

This paper has systematically investigated the characterizing features of a new variant of non-uniform helix antenna designated here as log-helix, and for which the non-uniformity is defined by a logarithmic variation along its axial length. Computational results suggest that when the logarithmic variation factor, β, assumes moderate values in the range 0.01 to 0.10, the log-helix radiates satisfactorily in the axial direction with better power gain in comparison with the conventional uniform helix. An exact equation describing the log-helix geometry facilitated the formulation of radiation integrals for the log-helix via the vector potential method. The distribution of current along the radiating structure when excited by a coaxial cable in conjunction with a ground plane of infinite extent is determined using the versatile method of moments together with the image theory.

A number of interesting outcomes were recorded for the 8-turn helix mounted on a ground plane of infinite extent, and utilized as the paper's candidate for use with investigations. Computational results for normalized $E_\vartheta(\vartheta, 0°)$ components of the radiation field patterns indicate that for given values of C_λ (or frequency) the main beam, in general, increases as β increases, though corresponding minor lobe levels become more prominent with decreasing values of logarithmic variation factor, β. On the other hand, the results reveal that for given values of the logarithmic variation factor, main beam becomes sharper with increasing frequency, as do the minor lobe levels. In the case of the normalized

$E_\phi(\vartheta, 0°)$ radiation-zone field patterns, the observed trend is that for given values of C_λ up to 1.10, main beam width sharpens with increasing values of β , and the associated minor lobes become less prominent. For values of $1.15 \leq C_\lambda = 1.30$, the trend is similar to that described earlier for the corresponding E_ϑ. Also, the normalized patterns for fixed values of β , exhibit the same characteristic behavior as described for the corresponding theta-components.

The performance of the log-helix was compared with that of a 4-turn exponential-helix, whose physical and operational parameters are specified in [7]. For the purposes of computational data, the finite ground plane in both cases was modeled by a wire grid, and the variation factors (β, C) were so selected as to make the axial profiles of both antennas as close as possible. The obtained computational results suggest that whereas the exponential helix, in general, has a better power gain performance than the log-helix, the latter's peak power gain is higher. On the other hand, and according to the computational results, the log-helix has a better axial ratio bandwidth performance than the exponential helix. It is worth remarking that the results reported in [1] and [10] indicated that when antenna non-uniformity is defined through diameter variation (rather than turns-spacing variation), the exponential helix has better power gain and axial ratio bandwidth performances. It should also be noted in that connection, that the profile of the logarithmic variation in [1] and [10] is a mirror reflection of that of the exponential helix.

One important conclusion from the comparative performance evaluation carried out in this paper is that for the log-helix, axial-ratio bandwidth is significantly enhanced, when the antenna's ground plane is of finite extent.

REFERENCES

[1] H. Elkamchouchi, A. Salem, "Helical antennas with nonuniform helix diameter," *18th National Radio Science Conference,* Mansonra University, Egypt, pp. B12(1-9), 2001.

[2] Y. Xiong, L. Huang, Y. Yu, J. Xiong, "Normal-mode helical antennas with near-field coupling: improving design flexibility," *IEEE Antennas and Propagation Magazine*, vol. 63, no. 1, pp. 75 – 85, 2021.

[3] H. Nakano, Y. Samada, J. Yamauchi, "Axial mode helical antennas," *IEEE Transactions on Mantennas and Propagation*, vol. 34, no. 9, pp. 1143-1148, 1986.

[4] K. Carver, "The helicone – a circularly polarized antenna with low sidelobe level," *Proceedings of IEEE*, vol. 55, no. 4, pp. 559, 1967.

[5] H. King, J. Wong, "Characteristics of 1 to 8 wavelength uniform helical antennas," *IEEE Transactions on Mantennas and Propagation*, vol. 28, no. 2, pp. 291-296, 1980.

[6] S. Fu, Y. Cao, Y. Zhou, S. Fang, "Improved low-profile helical antenna design for INMARSAT applications," *International Journal of Antennas and Propagation*, vol. 2012, 2012.

[7] C. Chen, E. Yung, B. Hu, S. Xie, "Axial mode helix antenna with exponential spacing," *Microwave and Optical Technology Letters*, vol. 49, no. 7, pp. 1525-1530, 2007.

[8] V. Kononov, C. Balanis, "Exponentially tapered helical antennas," *Proceedings of IEEE International Symposium on Antennas and Propagation,* pp. 2985-2988, 2007.

[9] K. Jimisha, S. Kumar, "Optimum design of exponentially varying helical antenna with non-uniform pitch profile," *Procedia Technology,* vol. 6, pp. 792-798, 2012.

[10] H. Elkamchouchi, A. Salem, "Effects of geometrical parameters, loading and feeding on nonuniform helical antennas," *19th National Radio Science Conference*, Alexandria, Egypt, pp. B4(1-11), 2002.

[11] J. Dinkic, D. Olcan, A. Djordjevic, A. Zajic, "Design and optimization of nonuniform helical antennas with linearly varying geometrical parameters," *IEEE ACCESS*, vol. 7, pp. 136855-136866, 2019.

[12] J. Dinkić, D. Olćan, A. Djordjević, A. Zajić, "High-gain quad array of nonuniform helical antennas," *International Journal of Antennas and Propagation*, vol. 2019, pp. 12, 2019.

[13] J. Dinkić, D. Olćan, A. Djordjević, A. Zajić, "Comparison of the optimal uniform and nonuniform lossy helical antennas," *2020 IEEE International Symposium on Antennas and Propagation and North American Radio Science Meeting*, Montreal, QC, Canada, pp. 423-424, 2020.

[14] R. Lovestead, A. Safaai-Jazi, "Optimum design of helical antennas by genetic algorithm," *Microwave and Optical Technology Letters*, vol. 62, no. 1, pp. 425-431, 2020.

[15] F. Gharakhili, "Design and fabrication of wide dual-band normal mode helical antenna," *International Journal of Engineering and Techniques*, vol. 4, no. 4, pp. 163-168, 2018.

[16] F. Mahmood, A. Al-Dalawei, "Design and implrmentation of a non-uniform helical antenna in frequency range of 450-850MHz for UHF television application," *Gihan Univesity-Erbil Scientific Journal*, vol. 3, no. 2, pp. 75-79, 2019

[17] J. Thaysen, K. Jakobsen, J. Appel-Hansen, "A logarithmic spiral antenna for 0.4 to 3.8GHz," *Applied Microwave and Wireless*, vol. 13, no. 2, pp. 32-45, 2001.

[18] E. Kreyszig, *Advanced Engineering Mathematics*, New Dehli: John Wiley, 1988.

[19] S. Adekola, A. Mowete, A. Ayorinde, "Performance characteristics of a dual-sense helical-beam antenna," *Progress in Electromagnetics Research Symposium*, Marrakesh, Morocco, pp. 573-576, 2011.

[20] A. Ayorinde, S. Adekola, A. Mowete, "Axial-mode performance characteristics of a thin-wire square helical antenna," *International Journal of Communications Antennas and Propagation*, vol. 8, no. 1, pp. 16-27, 2018.

[21] C. Balanis, *Antenna Theory: Analysis and Design*, New York: John Wiley, 1982.

[22] W. Stutzman, G. Thiele, *Antenna Theory and Design*, New York: John Wiley, 1981.

[23] J. Kraus, *Antennas*, New York: McGraw-Hill, 1988.